

Combination of dictionary learning by K-SVD and a colorimetric texture descriptor for improved identification of geological structures : Case of rocks

Joseph Wognin VANGAH¹, Sié OUATTARA¹, Alain CLEMENT², and Gbélé OUATTARA¹

¹URMI Electronique et Electricité Appliquées,
Institut National Polytechnique Felix Houphouët-Boigny (INP-HB), Côte d'Ivoire

²Laboratoire Angevin de Recherche en Ingénierie des Systèmes (LARIS),
Institut Universitaire de Technologie (IUT), Université d'Angers, France

Copyright © 2018 ISSR Journals. This is an open access article distributed under the *Creative Commons Attribution License*, which permits unrestricted use, distribution, and reproduction in any medium, provided the original work is properly cited.

ABSTRACT: In this paper, we propose a new representation of characteristics based on texture and color analysis for rock recognition. The proposed method combines the discriminating colour and texture characteristics of a rock image from a composite LBP descriptor to make automatic, fast and efficient rock identification. Indeed, the colorimetric texture descriptor ALBPCSF (Adjacent Local Binary Pattern based on Color Space Fusion) derives from the concatenation of the LBP texture characteristics and the color characteristics with the fusion of the two (02) colorimetric spaces RGB and HSV. In our methodology we first applied ALBPCSF on images of two (02) different families of rocks that are magmatic rocks and metamorphic rocks to produce colorimetric texture images then the K-SVD (K-Singular Value Decomposition) dictionary algorithm with a choice of suitable parameters is applied to said texture images produced to calculate a signature of the rocks from our image base. For dictionary learning the K-SVD method uses Orthogonal Matching Pursuit (OMP) as a sparse coefficient coding algorithm. The experimental results of the proposed approach on our image database show that the results of the proposed color LBP are relatively better than those with a grayscale or scalar LBP on the one hand and better than those of the direct K-SVD on the initial images on the other hand. The proposed strategy contributes significantly to improving the performance of automatic rock identification systems.

KEYWORDS: Rock Recognition, Color LBP, Scalar LBP, K-SVD, RGB, HSV, Color Texture, Errors.

1 INTRODUCTION

Dictionary learning and sparse representations have attracted the attention of many researchers in the areas of image processing, signal processing, computer vision and pattern recognition. The automatic identification of rocks, in the past decades, has sparked particular interest in pattern recognition and computer vision precisely, thanks to recurrent research published in this field [1]. This is motivated by the theoretical and experimental interests of geologists and experts in the field. However, the objective of rock recognition, whether manual or automatic, is to correctly and consistently identify rocks in order to minimize the subjectivity factor. As a result, rock reconnaissance has been a subject of active research and continuous investigation over the last ten years [1, 2]. Much progress has been made, but it is still difficult to develop a universal automated system capable of efficiently analyzing rock images because of the great variability and heterogeneity of their characteristics. And as with any classification task, feature extraction is paramount in the recognition process. This process in textural information extraction most often involves statistical, frequency and multi-scale methods. Recently, the Local Binary Pattern (LBP) originally proposed by Ojala et al. [4] for feature extraction, has gained reputation as a powerful texture descriptor and promoter in rock recognition [5, 7]. The main reasons why these approaches are becoming so popular are their simplicity on the feature extraction stage and their superiority in classification performance. The characteristics based on LBP proved to be highly discriminating due to different details found in the texture and to be effective due to its fast calculation. The most important properties of the LBP features are the tolerance against monotonic illumination changes, its robustness to scale and

orientation changes and the simplicity of its calculation. So far, many approaches have been developed and successfully used to improve rock recognition performance from microscopic images : K-NN methods [2, 3, 6], artificial neural networks (ANN) [1, 6, 10], SVM [11] and many others. Most of this work has been limited by the large size of the rock texture descriptors. In order to reduce the size of the descriptors, researchers use principal component analysis (PCA) [10] or a genetic algorithm [11] during the segmentation phase. However, the use of direct views of rocks for their identification has not yet been addressed. Current techniques are based on photo-interpretation, hence the particular interest of this paper. In the last decade, methods of parsimonious signal representation through K-SVD, have shown better performance in several research areas such as facial recognition [12], fingerprint recognition [13], super resolution [14], denoising [15], compression [16,30], classification [17] and many others. These performances have improved with dictionary learning [18]. However, the use of direct views of rocks for their identification has not yet been addressed. Current techniques are based on photo-interpretation, hence the particular interest of this paper. In the last decade, methods of sparse signal representation through K-SVD, have shown better performance in several research areas such as facial recognition [12], fingerprint recognition [13], super resolution [14], denoising [15], compression [16, 30], classification [17] and many others. These performances have improved with dictionary learning [18]. So far, many approaches have been developed and successfully used to improve the performance of rock recognition from microscopic images ; these are : the K- nearest neighbouring methods (K-NN) [2, 3, 6], artificial neural networks (ANN) [1, 6, 10], SVM [11] and many others. Most of this work has been limited to reducing the high dimensions of the rock texture descriptors by using principal component analysis (PCA) [10] or a genetic algorithm [11] during segmentation in order to reduce the size of the descriptors. However, the use of direct views of rocks for their identification has not yet been addressed. Current techniques are based on photo-interpretation, hence the particular interest of this paper. In the last decade, methods of sparse signal representation through K-SVD, have shown better performance in several research areas such as facial recognition [12], fingerprint recognition [13], super resolution [14], denoising [15], compression [16, 30], classification [17] and many others. These performances have improved with dictionary learning [18]. Moreover, in the literature studied, there is no at the moment application of the K-SVD method to rock recognition problems. This article aims to exploit the performance of this method in order to make rock reconnaissance from images of direct views of rock.

In the rest of this work, we will first present the texture and color descriptors in section II. Then in section III we describe the method of calculating and learning K-SVD dictionary, followed in section IV by the description of the proposed method. We end with Section V by presenting our results and their interpretations followed by perspectives.

2 TEXTURE AND COLOR DESCRIPTORS

Intuitively, color and texture produce the information we need to characterize a rock and distinguish one object from another.

2.1 COLOR DESCRIPTORS

Colour plays a fundamental rôle in distinguishing the content or objects constituting a scene or image given the analogy between the functioning of the human eye and patterns of human vision. It has been shown that colour characteristics achieve a higher success rate than gray- level features in image search and retrieval because colour characteristics contain sufficiently discriminating information [19, 20]. Therefore, the colors appearing in the images must be effectively characterized for a better classification of these images. In the field of image processing, a given color image I is définie as being a set of pixels each having three components red (R : Red), green (G : Green) and blue (B : Blue), which are the 03 primary colors, following scanning of the scene by a color camera or other dedicated digital device. In addition to the RGB color space, several other 03-dimensional color spaces exist. These are for example the HSV and CIElab spaces, introduced by Gonzales and Woods in 1993 [21]. These color spaces are obtained by combining the three primary colors, with some significantly different properties. The colour spaces used in our study are RGB and HSV. Indeed the HSV color space is motivated by the human vision system. In the HSV model, hue (H), saturation (S) and intensity (V) are considered separately. Hue and saturation define chrominance, while intensity or value specifies luminance [21]. Equations 1, 2, and 3 below show the conversion established by Gonzales and Woods between HSV or HSI and RGB color spaces.

$$H = \cos^{-1} \left\{ \frac{\frac{1}{2}[(R-G) + (R-B)]}{\left[(R-G)^2 + (R-B)(G-B) \right]^{1/2}} \right\} \quad (\text{Equation 1})$$

$$S = 1 - \frac{3}{(R+G+B)} [\min(R, G, B)] \quad (\text{Equation 2})$$

$$I = \frac{1}{3}(R+G+B) \quad (\text{Equation 3})$$

2.2 TEXTURE DESCRIPTORS

Like colour, texture is a fundamental factor in the perception of the environment and the recognition of objects. Unlike colour, texture remains an elusive concept that is difficult to define precisely and generically. The number of possible definitions given in the literature testify of this [22]. The literary definition of texture is the "spatial repetition of the same pattern in different directions of space". However, this explanation is sometimes considered insufficient since it is independent of, or does not meet, the needs of the human observer. For example, the texture of a fabric or a brick wall can satisfy this definition, which is not always the case for other textures. Texture has several discriminating visual aspects such as coarse, fine, grainy, regular or irregular appearance. Texture analysis methods for searching images have multiplied with the number of searches on the subject and can be grouped into 04 large families. Statistical methods, geometric or structural methods, methods based on probabilistic models and frequency methods can be distinguished. On this subject, Dounia A. 's thesis in 2014 [23] and the MPEG-7 standard in 2002 [24] provide an exhaustive account. Rock texture analysis consists in finding descriptive attributes that quantify the notions of granularity and directionality that are most important in this case and that are used by man to quantify rock textures. The nature of texture really conditions the approach to be used for its description and irregular and non-homogeneous textures are best characterized by statistical and model-based attributes with invariances to transformations caused by changes in observation conditions, such as rotation, translation, change in lighting conditions or change in spatial resolution. This is what justifies our choice of the LBP operator, which is one of the main texture descriptors based on spatial modelling used in colour image classification.

2.3 GENERAL INFORMATION ABOUT THE LBP DESCRIPTOR

In this section, we give only a brief introduction to the basic LBP method and one of its extensions. The reasons why we chose this family of texture descriptors from the vast plethora of features currently available are multiple. First, these techniques offer an excellent approach to analyzing texture at the microscopic level by analyzing the distribution of local texture elements (hence the name Local Binary Model), and in addition, they involve a low computational cost, making them attractive during the implementation of industrial applications. Thus, by using these techniques, a real-time processing could be achieved with a reasonable delay. Second, LBP techniques do not require complex optimization procedures, unlike many other methods. Third, the LBP and its variants are inherently invariant to changes in lighting intensity and monotonic image transformations and, finally, these characteristics have been shown to be effective and accurate in discriminant texture. Because of its characteristics, LBP is a well-known approach to texture analysis and has received substantial attention from image analysis practitioners. [7-9] make an excellent review of the method.

2.4 LOCAL BINARY PATTERN BASIC AND ITS VARIANTS

Texture is an important global descriptor for image analysis. The original LBP approach which is an excellent grayscale texture operator [4] has seen a significant breakthrough in texture analysis over previous methods applied specifically in facial, face and rock recognition. In this method, a texture image is represented with texture subparts called texture units. These units have 08 elements and are determined by comparing the pixels and their surroundings in the image. For an image, the LBP code is calculated by comparing the central pixel considered with the neighbouring pixels and the results of these comparisons are weighted and summed to give a binary number. Original LBP is defined as follows :

$$LBP_{P,R} = \sum_{i=0}^{P-1} s(p_i - p_c) \times 2^i, \quad s(x) = \begin{cases} 1 & \text{si } x \geq 0 \\ 0 & \text{otherwise} \end{cases} \quad (\text{Equation 4})$$

where p_c is the gray value of the central pixel, p_i is the gray value of the neighboring pixels, P is the number of neighboring pixels on the circle, R is the radius of the neighbor circle (see figure 3). LBP extracts the fundamental texture properties of the

local image. It is a texture descriptor based on the probability of elementary binary patterns (texels) appearing defined on a circular window. LBP is characterized by its tolerance to changes in lighting and illumination, its simplicity and speed of calculation that allow it to analyze complex textured images in real time. In order to extract the most fundamental structure and rotation invariance patterns of LBP, the uniform invariant and rotation operator $LBP_{P,R}^{riu2}$ [4] has been proposed and modeled as follows :

$$LBP_{P,R}^{riu2} = \begin{cases} \sum_{i=0}^{P-1} s(p_i - p_c) & \text{si } U(LBP_{P,R}) \leq 2 \\ p+1 & \text{otherwise} \end{cases} \quad (\text{Equation 5})$$

where the exponent *riu2* refers to the uniform invariant patterns of rotation that have a U value ($U \leq 2$). The uniformity measurement U corresponding to the number of transitions from 0 to 1 or from 1 to 0 between the successive bits in the circular representation of the binary code $LBP_{P,R}$ is defined as:

$$U(LBP_{P,R}) = |s(p_{p-1} - p_c) - s(p_0 - p_c)| + \sum_{i=1}^{P-1} |s(p_i - p_c) - s(p_{i-1} - p_c)| \quad (\text{Equation 6})$$

All non-uniform patterns are classified as a pattern for $LBP_{P,R}^{riu2}$. Mapping from to $LBP_{P,R}$ and $LBP_{P,R}^{riu2}$, which has (P + 2) separate output values, can be implemented with a search table.

In conclusion, most LBP variants focus on describing texture characteristics on grayscale images. However, the color characteristics are more discriminating than the gray-level characteristics [5, 19]. A review of these LBP color descriptors is done in [9]. In addition, the use of color characteristics combined with the relationships of the spatial structure of the previously exploited image makes it possible to improve the results efficiently for better recognition performance [25].

2.5 ADJACENT LOCAL BINARY PATTERN BASED ON COLOR SPACE FUSION (ALBPCSF)

The ALBPCSF operator proposed by Wang et al. in 2015 [25] is an improvement of LBP that takes into account color information in RGB and HSV color spaces. In addition, ALBPCSF adds spatial structure relationships to the characteristic vectors. Compared to existing improvements in LBP [7, 9], ALBPCSF successfully combines color functions and spatial structure relationships, making information of discriminating characteristics more abundant. The principle of this method is to extract texture characteristics when color characteristics and spatial structure relationships are not separated. First, the color characteristics of the different channels (RBG and HSV) are extracted precisely R, G, B and V then merged (R and V, G and V then B and V).

3 K-SVD METHODS

Sparse representations from dictionaries are techniques used in several fields such as statistics, telecommunications, medicine, image processing and are based on the principle of sparsity [26]. It is a question of representing all the declared data of a signal in vectors with a minimum of non-zero values based on a dictionary. Thus the model is simplified with fewer parameters and the characteristics of the image can be represented by linear combination of specific atoms of the dictionary. The minimization of the term sparsity is represented in the general form of p-standards with. This minimization is NP-difficult for pseudo standard [27, 30]. The optimization problem can be modeled as follows :

$$\min_{X,D} \|Y - DX\|_2^2 \text{ sous la contrainte } \forall i \|x_i\|_0 \leq T \quad (\text{Equation 7})$$

where $D = [d_1, d_2, \dots, d_N] \in \mathbb{R}^{m \times N}$ is a dictionary with N atoms and m indicates the number of attributes of each atom. $Y = [y_1, y_2, \dots, y_n] \in \mathbb{R}^{n \times n}$ is a learning set of n samples and $X = [x_1, x_2, \dots, x_n] \in \mathbb{R}^{n \times N}$ is the matrix of Y coefficients. T represents the number of non-zero or parsimony constraint elements.

There are two steps that occur simultaneously in the process of sparse representations : learning dictionary and sparse coding. These two steps are iterative. All the methods proposed in the literature follow these two steps. As for the step of sparse coding, it is generally performed by a Matching Pursuit algorithm which in our study is OMP [28] since it has proved effective with K-SVD [29]. As mentioned above, the OMP algorithm finds coefficients that are better correlated with signal

values given a fixed dictionary D. In addition, the OMP algorithm seeks an approximate solution through the selection and combination of atoms that minimize stress and quadratic error (5). This sparse coding step is represented by equation (8) below :

$$\min_{x_i} \|y_i - Dx_i\|_2^2 \text{ sous la contrainte } \|x_i\|_0 \leq T \quad (\text{Equation 8})$$

However, sometimes a fixed base is not able to provide the best representation of the y signal characteristics. Then, it is necessary to use special algorithms to adapt the dictionary values to the types of signals we process. This process is known as dictionary learning (combined with coefficient learning) and its purpose is to provide a precise basis for sparse representation. Sparse representation approaches as opposed to vector quantization (K-means) methods offer much more effective solutions and the effects of the dictionary on performance are examined in detail by authors in [26, 27, 29]. K-SVD (K- Singular Values Decomposition), which is a generalization of K-means, is an algorithm that adapts an over-complete D dictionary to the characteristics of a particular set of m learning signals $Y \in \mathbb{R}^{m \times n}$. This adaptive process consists of K iterations in which the dictionary is improved in order to obtain an accurate and sparse representation of the signals in Y. The K-SVD algorithm is one of the reference methods for learning the dictionary [30] in which the dictionary is adapted during the update of the coefficients:

$$\|Y - DX\|_2^2 = \left\| Y - \sum_{i=1}^m d_i x_i \right\|_2^2 = \left(\left\| Y - \sum_{i \neq j} d_i x_i \right\|_2^2 \right) - d_j x_j = \|R_j - d_j x_j\|_2^2 \quad (\text{Equation 9})$$

with d_j the column of the dictionary and x_j its corresponding coefficient, R_j the residue of the jth atom. The detail of the K-SVD process[30] is presented in the following algorithm through 4 steps :

K-SVD algorithm

Step 1: Initialize the normalized dictionary matrix $D^{(0)} \in \mathbb{R}^{m \times n}$

Step 2 : Stop iteration if the change $\|Y - DX\|_2^2$ is small enough, otherwise, go on the next iteration.

Step 3 : use OMP to compute the representation vectors $x_i, i=1, 2, \dots, n \min_{x_i} (\|y_i - Dx_i\|_2^2) \text{ subject to } \|x_i\| \leq T_0$

Step 4 : Update each column in D, k =1, 2, ..., N by :

- (1) Define the group of examples that use $d_k, \omega_k = \{i | 1 \leq i \leq n, x_{i(k)} \neq 0\}$.
- (2) Compute the overall representation error matrix $E_k = Y - \sum_{j \neq k} d_j x^j$
- (3) Restrict E_k by choosing the columns corresponding to those elements which initially used d_k in representation, then obtain E_k^R .
- (4) Through SVD, $E_k^R = U \Delta V^T$. Select the updated dictionary column d_k as the first column of U , and $x_R^k = \Delta(1,1) \cdot v_1$.

4 PROPOSED METHOD

The characterization of the rock recognition is based here on the reconstruction error parameter ϵ defined and estimated in the K-SVD algorithm [30]. The principle of the proposed approach is presented in Figure 1 below. Three reconstruction errors are calculated in different ways. The first error named ϵ_{Direct} is calculated by directly applying the K-SVD algorithm to each direct view image of the rocks in the image base. The second error noted at ϵ_{LBP} is obtained first by applying the LBP algorithm to each image in the database producing texture images followed by applying the K-SVD algorithm to the texture images. The third error noted at $\epsilon_{\text{FLBPCouleur}}$ is calculated in the same way as the second error except that the LBP is replaced by the color texture algorithm (ALBPCSF) [25]. We opted for a customization of the ALBPCSF algorithm by considering two central pixels

paired with a radius of one (1) pixel and a distance of two (2) pixels between the two pixel centers of even LBP. Indeed, four (4) related neighbours are considered. Considering the first pixel center LBP (i, j), the second matched LBP has pixel center (i, j+3). Let I1 and I2 be two images from two (2) spectral channels RGB and HSV. Let T11 and T12 be the matrices, each containing the four (4) centered neighbors of the even LBP from image I1, and T21 and T22 the matrices, each containing the four (4) neighbors of the even LBP from image I2. A binarization of matrices T11, T12, T21 and T22 is carried out and stored in matrices TU and TL defined by formula (7) and (8) below :

$$T_U = \begin{cases} 1 & \text{si } T_{11}(k) > 0 \text{ et } T_{21}(k) > 0 \\ 0 & \text{otherwise} \end{cases} \quad (\text{Equation 10})$$

$$T_L = \begin{cases} 1 & \text{si } T_{12}(k) < 0 \text{ et } T_{22}(k) < 0 \\ 0 & \text{otherwise} \end{cases} \quad (\text{Equation 11})$$

$$\text{Codage}U = \sum_{i=0}^3 T_U(k) \times 2^k \quad (\text{Equation 12})$$

$$\text{Codage}L = \sum_{i=0}^3 T_L(k) \times 2^k \quad (\text{Equation 13})$$

Then decimal coding is performed on the TU and TL matrices to obtain scalars named CodageU and CodageL expressed by formulae (12) and (13), varying between 0 and 15 with finally the combination of their pair varying between 0 and 255. Let be a color image I of color component I_R, I_G and I_B in the initial RGB space. Its transformation in HSV space gives rise to the colorimetric components I_H, I_S and I_V. Component I_V is then matched with components I_R, I_G and I_B. To these pairings, the ALBPCSF algorithm is applied to obtain a U-type color image noted ImageU and an L-type color image noted ImageL. To finish we retained the U type color image, the only one containing exploitable information for our case. It is to this image that we applied the K-SVD algorithm to obtain the colorimetric error noted at $\epsilon_{fLBP \text{ color}}$.

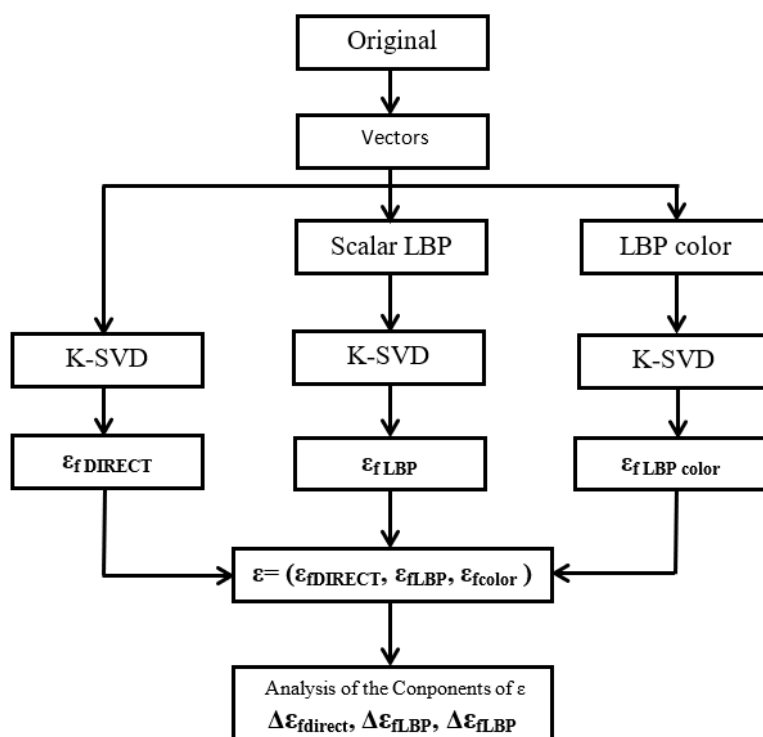


Fig. 1. Organization chart of the principle of the proposed approach

5 RESULTS AND DISCUSSION

This section presents the detailed experimental results of the proposed approach. Eleven direct view images of different magmatic and metamorphic family rocks from our database are used in this paper to highlight the performance of our method. These are: granite, granodiorite, gabbro, schists, migmatite, eclogite, cornea and cipolin. These images, captured in the RGB color space, once taken were saved in TIFF format, with a resolution of 256*256. We have grouped the images into 4 classes (class 1, class 2, class 3, class 4) according to certain textural and visual colorimetric similarities as presented in figure 2 below.



Figure 2: Direct view rocks images of different classes

In class 4 of figure 2, the rock textures are fairly regular with low granularity (homogeneous and microgranular structure) but are different in directionality. However, the directionality in the textures of classes 1, 2 and 3 are clearly not homogeneous with textures showing a variation in coarse grain structures (high granularity or macrogranularity). In [31], Lepisto et al. confirm that the classification of rock textures takes into account grain size (high granularity or not), directionality and colorimetric properties.

The execution of our program under MATLAB is realized with a computer HP Notebook Processor Intel(R) Core(TM) i5-7200U CPU @ 2.50GHz, 2701 MHz, 2 core(s), 4 processor(s) logic(s), graphics card Radeon with a Windows 10 system company.

For the classification task, we used direct view RGB color rock images of dimensions 256x256x3. By applying the scalar ALBPCSF and LBP algorithms, we obtain color texture images and grayscale texture images as shown in Figure 3 below. This figure 3 is divided into 4 tables noted Figures 3a, 3b, 3c and 3d, presenting the 4 classes (class 1, class 2, class 3 and class 4) shown above.

Figure 3a. images of class 1

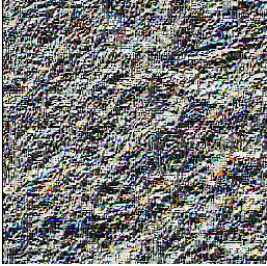
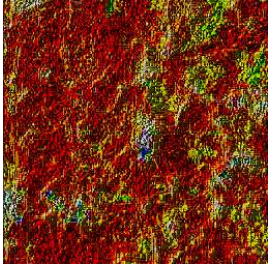
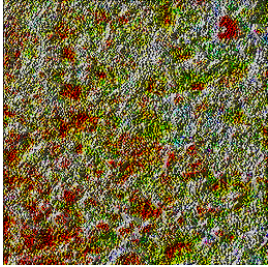
Granit			
	Original image	LBP image in gray level	Color texture image
Granodiorite			
	Original image	LBP image in gray level	Color texture image

Figure 3b. images of class 2

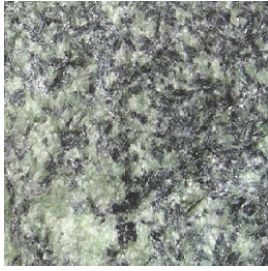
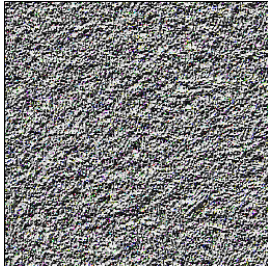
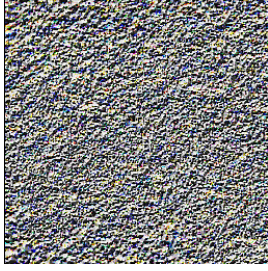
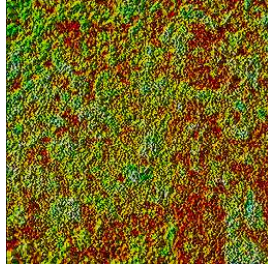
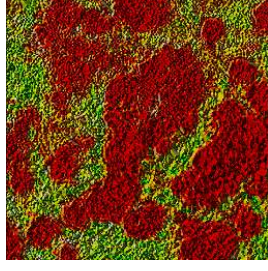
<i>Schist951</i>			
	Original image	LBP image in gray level	Color texture image
<i>Schist31</i>			
	Original image	LBP image in gray level	Color texture image
<i>Cipolin</i>			
	Original image	LBP image in gray level	Color texture image

Figure 3c. images of class 3

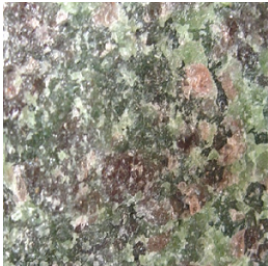
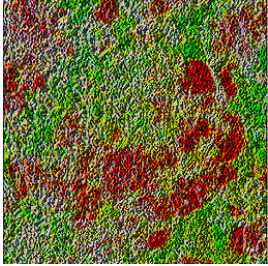
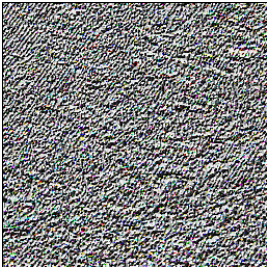
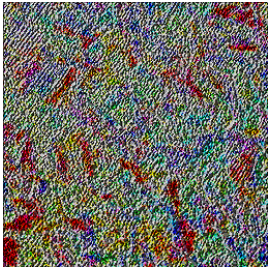
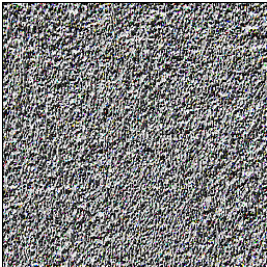
<i>Eclogite</i>			
	Original image	LBP image in gray level	Color texture image
<i>Gabbro</i>			
	Original image	LBP image in gray level	Color texture image
<i>Migmatite</i>			
	Original image	LBP image in gray level	Color texture image

Figure 3d. images de la classe 4

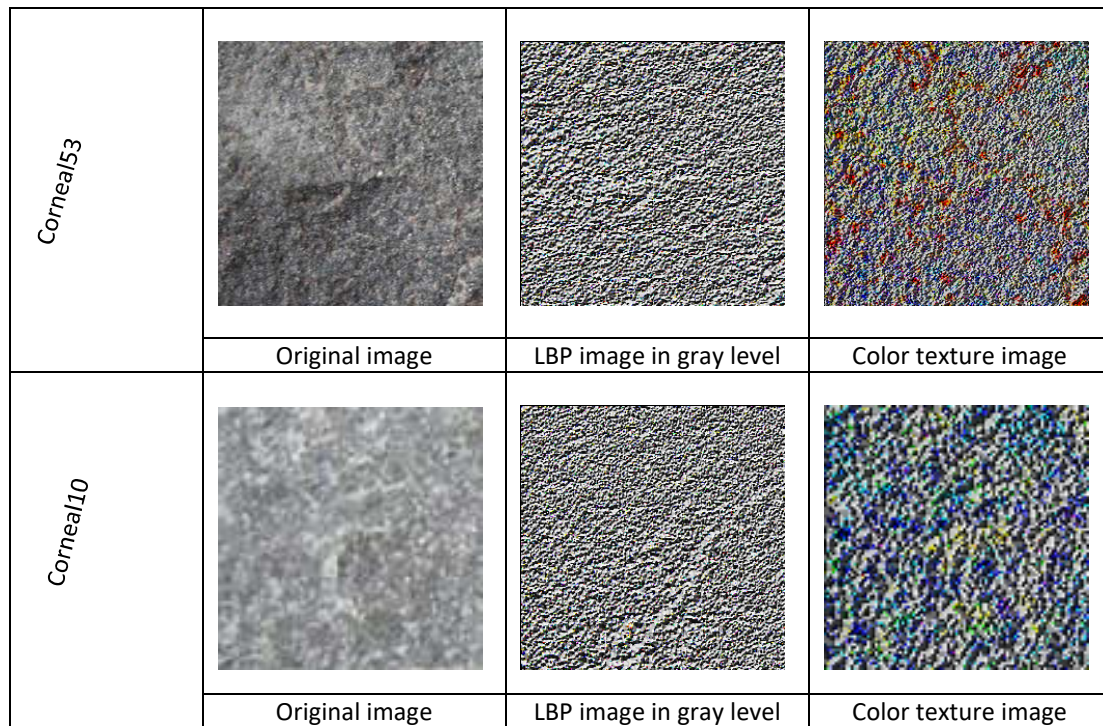


Figure 3. Color texture images and grayscale images

Our classification method is an unsupervised calculation and learning method. The reconstruction errors calculated for each type of image texture by our approach are presented in different tables (table 1, table 2, and table 3) followed by analysis and interpretation of the data. Table 1 presents the results of the calculation of the different reconstruction errors. By analyzing the values of ϵ for the different methods (K-SVD, K-SVD_LBP and K-SVD_ALBPCSF), each method plays an important rôle in rock classification. This is justified by the heterogeneity of their characteristics and confirms the difficulties encountered in manual classification. Indeed, column 4 of Table 1 reveals that $\epsilon_{LBP\ standard} = 16.673$ for cornea53 is the lowest value before the other values in this column. These values compare the fine texture of the cornea53 with the granoblastic texture of the other rocks (magmatic and meamorphic) in the table1 and confirm the effectiveness of the LBP operator on the texture of the rocks as revealed [7]. Also the 3 lower values in the 3rd column correspond to images where light colors are dominant. The second column (ϵ_{DIRECT}) shows a geometric similarity of the grains with on one side lower values for strong granularities and on the other side higher values when the grains are smaller.

Table 1. Calculated reconstruction errors

Rock images	ϵ_{DIRECT}	$\epsilon_{LBP\ colour}$	$\epsilon_{LBP\ standard}$
Granit	1.1694	16.6968	18.9879
Granodiorite	1.9671	20.2557	19.8687
Gabbro	2.2284	19.6160	18.3108
Cipolin	1.5716	16.9661	20.0325
Migmatite	1.9809	19.3918	19.2034
Eclogite632	3.1678	19.8531	19.1813
Corneal53	2.0213	19.8962	16.673
Corneal10	2.4666	20.0042	18.0263
Schist31	2.2651	17.4324	18.3735
Schist951	4.2882	20.5470	18.4481
Schist936	3.0896	20.3171	17.0726

Except for granite, Cipolin and Schist31, the values of the color LBP errors are higher than those of the standard LBP errors but with much smaller error variations for these 03 images, showing a great similarity between these three rocks. It also confirms that the color characteristics have been taken into account and are discriminating as indicated in [5]. Also in these images, grainy and granoblastic textures are more revealed.

The color LBP values show similarity in color and reveal gray textures with similar orientations with higher crystallization temperatures but some differences exist as in the case of corneal10.

The values of LBP colors show a similarity in texture (microlitic texture) but nevertheless show a very large difference between the minerals existing in these rocks.

In Table 2 below, the reconstruction error variations are calculated by rock family in order to identify possible similarities between the rocks.

Table 2. Analysis of error variations of rocks of identical families

Rock type	Rocks of the same family	$ \Delta\epsilon_{LBPcolour} $	$ \Delta\epsilon_{LBP} $	$ \Delta\epsilon_{DIRECT} $
Magmatic rocks	Granite - Gabbro	2.6480	0.6771	1.0590
	Granite – Granodiorite	3.5589	0.8808	0.7977
	Gabbro - Granodiorite	0.6397	1.5579	0.2613
Métamorphic Rocks	Schist31 – Corneal53	2.4638	1.7005	0.2438
	Corneal10- Schist951	0.5428	0.4218	1.8216
	Corneal10 - cipolin	3.0381	2.0062	0.8950
	Schist951 - Cipolin	3.5809	1.5844	2.7166
	Schist31 – Schist936	2.8847	1.3009	0.8239
	Migmatite – Corneal53	0.5044	2.5304	0.0404
	Schist31-Schist951	3.1146	0.0746	2.0231
	Corneal10-Corneal53	0.1080	1.3533	0.4453
	Migmatite – Corneal10	0.6124	1.1771	0.4857
	Migmatite – Cipolin	2.4257	0.8291	0.4093
	Migmatite -Schist31	1.9594	0.8299	0.2842
	Migmatite -Schist951	1.1552	0.7553	2.3073
	Migmatite -Schist936	0.9253	2.1308	1.1089
	Cipolin – Schiste1	0.4663	1.6590	0.6935
	Cipolin – Schist951	3.5809	1.5844	2.7166
Cipolin – Schist936	3.3510	2.9599	1.5180	

The results of this table above show the existence of structural similarities (granular, granoblastic and microlitic texture) between rocks belonging to the same family (magmatic or metamorphic). As far as magmatic rocks are concerned, these results show a particular relationship between granite and granodiorite from the structural point of view, with a large difference in colour reflecting a difference in minerals. For Granodiorite and Gabbro, there is a visible difference in texture with however a somewhat similar textural orientation while there is an average similarity in color and a difference in textural orientation of Gabbro and Granite.

The Migmatite, Corneal10 and Schist936 rocks show a certain similarity in colour, reflecting the presence of common minerals, but with a great similarity in structure between the first two rocks and the Schist31. Also between corneal53 and migmatite where there is some resemblance with certainly a very great difference in color with corneal53. Table 3 below shows the reconstruction error variations calculated for different rock families in order to identify possible similarities between these rocks.

Table 3. Analysis of error variations of rocks of different families

Roches de familles différentes				
Roches magmatiques	Roches métamorphiques	$ \Delta\varepsilon_{LBP} $	$ \Delta\varepsilon_{DIRECT} $	$ \Delta\varepsilon_{LBPcouleur} $
Granite	Migmatite	0.2155	0.8115	2.6950
	Schiste31	0.6144	1.0957	0.7356
	Cipolin	1.0446	0.4022	0.2693
Gabbro	Cornéenne10	0.8926	0.2382	0.3882
	Schiste951	0.1373	2.05598	0.9310
	Migmatite	0.8926	0.2475	0.2318
	Cornéenne53	0.8926	0.2071	0.2802
	Eclogite	0.8705	0.9394	0.2371
Granodiorite	Cornéenne10	1.8424	0.4995	0.2515

Analysis of the variations shows that there are very great similarities in colour and structure or texture between rocks of different families, thus expressing the presence of identical minerals found in these rocks. This confirms the fact that some metamorphic rocks are of magmatic origin (e.g. Eclogite, Migmatite and Schiste 951). More precisely, there is a strong similarity in structure (directionality and orientation) and in colour between Gabbro and metamorphic rocks (dark colour). This table exalts the existence of a very great regularity between visual recognition and our proposed algorithm.

Table 4. Analysis of the error variations of the rocks of the same families with three chosen metrics: the average (Moy), the maximum (Max) and the L2 distance

Rock type	Rocks of the same family	$ \Delta\varepsilon_{fLBPcouleur} $	$ \Delta\varepsilon_{fLBP} $	$ \Delta\varepsilon_{fDIRECT} $	Mesure 1 : Moy	Mesure 2 : Max	Mesure 3 : L2 Distance
Magmatic Rocks	Granit - Gabbro	2.6480	0.6771	1.0590	1,4614	2,648	2,9312
	Granit – Granodiorite	3.5589	0.8808	0.7977	1,7458	3,5589	3,7520
	Gabbro - Granodiorite	0.6397	1.5579	0.2613	0,8196	1,5579	1,7043
Metamorphic rocks	Schist31 – Corneal53	2,4638	1,7005	0,2438	1,4694	2,4638	3,004
	Corneal10- Schist951	0,5428	0,4218	1,8216	0,9287	1,8216	1,9470
	Corneal10 - cipolin	3,0381	2,0062	0,895	1,980	3,0381	3,7491
	Schist951 - Cipolin	3,5809	1,5844	2,7166	2,6273	3,5809	4,7658
	Schist31 – Schist936	2,8847	1,3009	0,8239	1,6698	2,8847	3,270
	Migmatite – Corneal53	0,5044	2,5304	0,0404	1,0251	2,5304	2,5805
	Schist31-Schist951	3,1146	0,0746	2,0231	1,7374	3,1146	3,7147
	Corneal10-Corneal53	0,108	1,3533	0,4453	0,6355	1,3533	1,4288
	Migmatite – Corneal10	0,6124	1,1771	0,4857	0,7584	1,1771	1,4130
	Migmatite – Cipolin	2,4257	0,8291	0,4093	1,2214	2,4257	2,5959
	Migmatite -Schist31	1,9594	0,8299	0,2842	1,0245	1,9594	2,1468
	Migmatite -Schist951	1,1552	0,7553	2,3073	1,4059	2,3073	2,6886
	Migmatite – Schist936	0,9253	2,1308	1,1089	1,3883	2,1308	2,5741
	Cipolin – Schist31	0,4663	1,659	0,6935	0,9396	1,659	1,8576
	Cipolin – Schist951	3,5809	1,5844	2,7166	2,6273	3,5809	4,7658
Cipolin – Schist936	3,351	2,9599	1,518	2,6096	3,351	4,7217	

Table 5. Analysis of the error variations of the rocks of different families with the 3 metrics: Average (Moy), the maximum (Max) and the L2 distance

Rocks from different families							
Magmatic rocks	Metamorphic rocks	$\Delta\epsilon_{FLBP}$	$\Delta\epsilon_{DIRECT}$	$\Delta\epsilon_{ALBPCSF}$	Mesure1 :Moy	Mesure 2 : Max	Mesure 3 : L2Distance
Granite	Migmatite	0,2155	0,8115	2,695	1,2407	2,695	2,8227
	Schist31	0,6144	1,0957	0,7356	0,8152	1,0957	1,4557
	Cipolin	1,0446	0,4022	0,2693	0,5720	1,0446	1,1513
Gabbro	Corneal10	0,8926	0,2382	0,3882	0,5063	0,8926	1,0021
	Schist951	0,1373	2,05598	0,931	1,0414	2,056	2,2611
	Migmatite	0,8926	0,2475	0,2318	0,4573	0,8926	0,9548
	Corneal53	0,8926	0,2071	0,2802	0,4600	0,8926	0,9582
	Eclogite	0,8705	0,9394	0,2371	0,6823	0,9394	1,3025
Granodiorite	Corneal10	1,8424	0,4995	0,2515	0,8445	1,8424	1,9254

Analysis of Tables 4 and 5 shows that:

Gabbro, Granodiorite and Corneal10 have a similar relationship of color. This is translated as the Mean metric shown in Tables 4 and 5 above.

The metamorphic rocks (Corneal53, Corneal10 and Migmatite) have a similar relationship of color with Gabbro and between them, confirmed by the metric Mean of the same tables. However, they have very little similarity in colour with Schiste951 and Eclogite.

As far as the relationship between magmatic rocks is concerned, slight similarities in structure (opposition of grain shapes: small and large grains) exist between them, but with a higher similarity in colour between Gabbro and Granodiorite, confirmed by the Medium metric. The similarities of directionality and orientation in texture are not too visible in these rocks and for this purpose the values of the metrics: Max and L2 Distance confirm it.

The metamorphic rocks studied here present in their great majority similarities of structure (small and fine granularity), similarities of directionality, orientation and more significantly of color with Gabbro. These visual properties are highlighted by the metrics (Mean and Max).

In addition, other metamorphic rocks such as Schist31, Cipolin and Migmatite have average colour similarities with low similarities of granularity and directionality with granite with reference to the values of the Metrics Mean and Max in tables 4 and 5 above.

6 CONCLUSION

In this article, we applied for the first time to our knowledge this new image feature descriptor called ALBPCSF to direct view rock images. In the classification of rock texture images, it has been beneficial to combine texture characteristics and color information in order to make a better classification. However, it should be noted that rock textures are very difficult to identify for two reasons firstly because of their very varied, irregular and heterogeneous nature and secondly because metamorphic rocks have undergone important transformations of a purely structural or purely mineralogical nature, or of a structural and mineralogical nature at the same time. ALBPCSF has compensated for the LBP deficiency and is more suitable for colour image classification. In principle, we merged RGB and HSV color spaces to obtain color information and spatial structure relationships to improve classification performance. The mean metric better describes the color similarity in the images while the structure and directionality/orientation similarities are decied by the Max and the distance L2. The color descriptor allows to better differentiate or to find a similarity between the rocks of the same families and those of the different families. The results of the different tables presented showed that the performances of the ALBPCSF + K-SVD algorithm are better than those with K-SVD. Indeed, we notice a good concordance between the identification or visual recognition and the response of our method confirming the good choice of rock characteristics and the methods used for their extraction. Moreover, the difficulties encountered result from the important diversification of rock properties due to the difference linked to their genesis (since their original formation). These same difficulties have been mentioned in the analysis or manual recognition. In perspective, we plan to introduce Gabor filters and/or wavelets to further refine our results.

REFERENCES

- [1] H. Izadi, J. Sadri, M. Bayati, "An intelligent system for mineral identification in thin sections based on a cascade approach", *Computers & Geosciences*, Vol. 99, pp. 37–49, 2017.
- [2] M. Mlynarczyk, A. Gorszczyk, and B. Slipek, "The application of pattern recognition in the automatic classification of microscopic rock images," *Computers and Geosciences*, Vol. 60, pp. 126-133, 2013.
- [3] M. Ladniak and M. Mlynarczyk, "Search of visually similar microscopic rock images," *In comput. GEOSCI*, Vol. 19, pp. 127-136, 2014.
- [4] T. Ojala, M. Pietikainen and T. Maenpaa, "Multiresolution gray-scale and rotation invariant texture classification with local binary patterns," *IEEE Transactions on Pattern Analysis and Machine Intelligence*, vol. 24, no. 7, pp. 971-987, 2002.
- [5] F. Bianconi, E. Gonzalez, A. Fernandez and S. A. Saetta "Automatic Classification of granite tiles through colour and texture features," *Expert Systems with Applications*, vol. 39, no.12, pp. 11212-11218, 2012.
- [6] M. Mlynarczyk, M. Skiba, "The Application of Artificial Intelligence for the Identification of the Maceral Groups and Mineral Components of Coal", *Computers and Geosciences*, Vol. 103, pp. 133-141, 2017.
- [7] A. Fernandez, O. Ghita, E. Gonzalez, F. Bianconi and P. F. Whelan, "Evaluation of robustness against rotation of LBP, CCR and ILBP features in granite texture classification," *Machine Vision and Application, Springer*, no. 22, pp. 913-926, 2011.
- [8] L. Nanni, A. Lumini and S. Brahmam, "Survey on LBP based texture descriptors for classification", *Expert Systems with Applications*, Vol. 39, pp. 3634-3641, 2012.
- [9] S. Banerji, A. Verma and C. Liu, "Novel color LBP descriptors for scene and image texture classification", in *Proceedings of the 15th International Conference on Image Processing, Computer Vision, and Pattern Recognition*, Las Vegas, Nevada, pp. 537–543, 18-21 July 2011.
- [10] N. Singh, T. N. Singh, A. Tiway and K. M. Sarkar, "Textural identification of basaltic rock mass using image processing and neural network," *Computer and Geosciences*, Vol. 14, pp. 301- 310, 2010.
- [11] S. Chatterjee: Vision-based rock-type classification of limestone using multiclass support vector machine. *Applied Intelligence*, Vol. 39, pp. 14-27, 2013.
- [12] G. Zhang, H. Sun, Z. Ji, G. Xia, L. Feng and Q. Sun, "Kernel dictionary learning based discriminant analysis," *In J. Vis. Commun. Image R.*, Vol. 40, pp. 470-484, 2016.
- [13] G. Shao, Y. Wu, A. Yong, X. Liu, and T. Guo, "Fingerprint Compression Based on Sparse Representation," *IEEE transactions on image processing*, Vol. 23, No. 2, pp. 489-50, 2014.
- [14] J. Yang, J. Wright, Y. Ma, T. Huang, "Image super-resolution via sparse representation," *IEEE Trans. Image Process.* Vol. 19, no. 11, pp. 2861–2873, 2010.
- [15] M. Elad, M. Aharon, Image denoising via sparse and redundant representation over learned dictionaries, *IEEE Trans. Image Process.* Vol. 15, no. 12, pp. 3736–3745, 2006.
- [16] J. Aghaei Mazaheri, C. Guillemot, C. Labit. Learning a tree-structured dictionary for efficient image representation with adaptive sparse coding. *ICASSP*, 2013
- [17] S. Chan Wai Tim, M. Rombaut and D. Pellerin. "Multi-layer Dictionary Learning for Image Classification". In : *Advanced Concepts for Intelligent Vision Systems*. 2016.
- [18] I. Tomic and P. Fossard : Dictionary learning, *IEEE Signal Processing Magazine*, Vol. 28, pp. 27–138, 2011.
- [19] E. Gonzalez, F. Bianconi, M. X. Alvarez, S. A. Saetta, "Automatic characterization of the visual appearance of industrial materials through colour and texture analysis: An overview of methods and applications", *Hindawi Publishing Corporation Advances in Optical Technologies*, Vol. 2013, pp. 11, 2013.
- [20] C. Liu and J. Yang, "ICA color space for pattern recognition", *IEEE Trans. on Neural Networks*, vol. 20, no. 2, pp. 248-257, 2009.
- [21] R. G. Gonzalez and R. E. Woods, Edition. S. I. Digital Image Processing using MATLAB, 2009.
- [22] R. M. Haralick, "Statistical and Structural approach to texture," *Proceeding of the IEEE*, Vol. 67, no. 5, May 1979.
- [23] Dounia Awad. Towards a perceptual object recognition system. Computer vision and pattern recognition. *PhD thesis at the Université de la Rochelle, at the Laboratoire Informatique, Image, Interaction Pole Sciences et Technologies*, 2014.
- [24] B.S. Manjunath, P. Salembier, T. Sikora, Introduction to MPEG-7: Multimedia Content Description Interface, Wiley, Chichester, 2002.
- [25] S. Wang, D. Huang, H. Jia, D. Liu and B. B. Dickson, "Adjacent Local Binary Patterns Based on Color Space Fusion for Color Image Classification", *Journal of Fiber Bioengineering and Informatics*, vol. 8, no. 4, pp. 783-790, 2015.
- [26] J. Mairal, F. Bach, J. Ponce, "Sparse modeling for image and vision processing", *Found. Trends. Comput. Graph. Vis.* Vol. 8, no. 2-3, pp. 85-283, 2014.
- [27] M. Elad, "Sparse and redundant representations : from theory to applications in signal and image processing, 1st, Springer Publishing company. Incorporated, 2010.

- [28] Y. C. Pati, R. Rezaifar, P. Krishnaprasad, "Orthogonal matching pursuit : Recursive function approximation with applications to wavelet decomposition". *Conference Record of The 77th Asilomar Conference on Signals, Systems and Computers, IEEE*. pp. 40–44,1993.
- [29] R. Rubinstein, A. M. Bruckstein, M. Elad, Dictionaries for sparse representation modeling, *Proc. IEEE*. Vol. 98, no. 6, pp. 1045–1057, 2010.
- [30] M. Aharon, M. Elad, A. Bruckstein : K-SVD : An algorithm for designing over-complete dictionaries for sparse representation. *IEEE T. Signal Processing*. Vol. 54, no. 11, pp. 4311–4322, 2006.
- [31] L. Lepistö, L. Kunttu and A. Visa, "Rock image classification using Color features in Gabor space", *Journal of Electronic Image*, Vol. 14, no. 4, pp. 1-3, 2005.